

Electronic supplement to

How steady are steady-state mountain belts? – a re-examination of the Olympic Mountains by Michel et al.

S1 Details for thermochronometric dating

S1.1 Identifying outlier single-grain ages of (U-Th)/He dating

In the following we explain our procedure for deciding which apatite and zircon single grains are excluded from sample age calculation. The entire (U-Th-Sm)/He dataset of our analysed apatite and zircon single grains can be found in Tables S1 and S2, respectively. Calculating sample cooling ages for AHe and ZHe from single-grain ages was complicated in some samples for two main reasons: (1) Cooling ages for the sedimentary rocks from the Olympic Mountains can be unreset, (i.e., the single-grain ages can exhibit cooling ages representative of the sediment source terrains), and (2) The geologic uncertainty for (U-Th-Sm)/He dating is often larger than the analytic uncertainty, which can lead to over-dispersed single-grain ages (e.g., Fitzgerald et al., 2006; Flowers and Kelley, 2011).

In order to determine whether a sample contains outliers or is unreset, we used the following protocol. Samples where all single-grain ages are older than the depositional age of the sample or where single-grain ages show a large spread and do not overlap within analytical uncertainty (e.g., apatites of sample OP1560 or zircons of sample OP1557; Table S1 and S2), are considered as unreset samples. If samples pass this first test, we identify possible outliers by checking whether single-grain ages overlap within 2SD. Anomalously old single grains are considered outliers and excluded from sample cooling age calculations (e.g., single apatites of samples OP1552 and OP1553; Table S1). Furthermore, if single-grain ages of a sample are disputable, we consider information

from the higher closure temperature system of the sample or other samples collected along the same elevation transect. For example, if the ZHe age of a certain sample is reset or if AHe ages of samples at higher or lower elevation have concordant ages, we consider the AHe system of that sample to be reset. This applies to AHe ages of samples OP1555, OP1572 and OP1576. For samples OP1572 and OP1576, we take the youngest apatite single-grain age as sample cooling age (due to the low high-quality apatite yield).

S1.2 Further information for FT dating

AFT and ZFT single-grain data are reported as additional files in Tables S3 and S4.

S2 Additional information for thermo-kinematic modeling

During thermo-kinematic modeling, we used a time step interval of 1 Myr (as reported in Figure 5). Using sample OP1513 as an example, we performed sensitivity tests for different time steps (Figure S1). We considered four additional intervals of 2 Myr, 3 Myr, 0.5 Myr, and an interval, where the duration is variable and depends on the time between the different thermochronometer ages of the sample.

For sample OP1513, the exhumation rate history using a 1 Myr time step (Fig. S1d) is as follows: High rates (~ 1 km/Myr) are observed between 10–12 Ma, slow rates (< 0.5 km/Myr) between 4–10 Ma, and an increase in rates to values > 1 km/Myr starting at 2 Ma. Simulations using the four additional time steps (Fig. S1a-d) result in a similar history of “high-low-high” exhumation rates as the model with the 1 Myr time step. However, the timing of an increase or decrease in exhumation rates occurs at a multiple of 0.5 Myr, 2 Ma or 3 Ma, respectively. If the respective time step is long (e.g., for the 3 Myr simulation or for some time steps in S1c), then the corresponding exhumation rate

has to be lower compared to the 1 Myr or 2 Myr simulations, in order to result in the same amount of exhumation during a given time span. Furthermore, for long time steps, the uncertainty for a given time step is reduced (grey area around the mean exhumation rate in Fig. S1).

The simulation with the 0.5 Myr time step (Fig. S1d) suggests a very fine temporal resolution and, in particular in the time interval between 3 Ma and 0 Ma, several spikes occur in the mean exhumation rate curve. It is important to consider that for most of our thermochronometer ages the respective uncertainties are between 0.5 Myr and 1.5 Myr. Hence, the suggested spikes in exhumation rates using a time step of 0.5 Myr are not well resolvable with our thermochronometry data. Although we did not test time steps shorter than 0.5 Myr, we suspect to observe a similar pattern of exhumation rate spikes. Due to the reason outlined above, we believe that models with a time step significantly shorter than 1 Myr pretend a temporal resolution that on the other hand is not resolved by our thermochronometry data, placing a minimum threshold on a reasonable time step.

In general, meaningful histories can only be derived for the time span covered between today and the oldest thermochronometer age of a sample. From all of our modeled samples, sample OP1513 has the oldest ZHe age (10.2 Ma). Therefore, it has the longest exhumation history resolved by our modeling and a time step of 3 Myr still results in a meaningful exhumation history (i.e., it has four time steps). Sample OP1533 (AFT/ZHe ages of ~6 Ma) has a much shorter time span resolved, hence a time step interval of 3 Myr would result in two time steps, and in case of a 2 Myr interval in three time steps. So, longer time steps place a limitation on the information obtained from

exhumation histories for particularly young samples and model runs with longer time steps seem not to be feasible for some of the considered samples

A variation in exhumation rate can only occur at the beginning of a time step in our simulations. So, for the simulation where the duration of the time steps is controlled by the thermochronometer ages of the respective sample (Fig. S1c), the derived pattern of exhumation rates depends on the actual cooling ages. This impacts the direct comparison between the different samples, because a possible decrease or increase in exhumation rate occurs at different times, compared to simulations, where all samples use the same, fixed time step.

Based on the observations above, the general history of exhumation rates seems not to be sensitive to the time step. We believe that a time step interval of 1 Myr is the best trade-off between the investigated time steps and should yield reasonable exhumation rate patterns for all of our samples, which can have very different thermochronometer ages. Although the exhumation rate histories shown in Figure 5 have step-like patterns and suggest a high temporal sensitivity due to the 1 Myr time step, the interpretation of these histories should be based on a smoothed pattern, as we used in Figure 8. Furthermore, although we calculate the mean exhumation rate for each time step (red lines in Fig. 5 and Fig. S1), the respective uncertainty of this mean exhumation rate should also be considered (grey areas in Fig. 5 and Fig. S1).

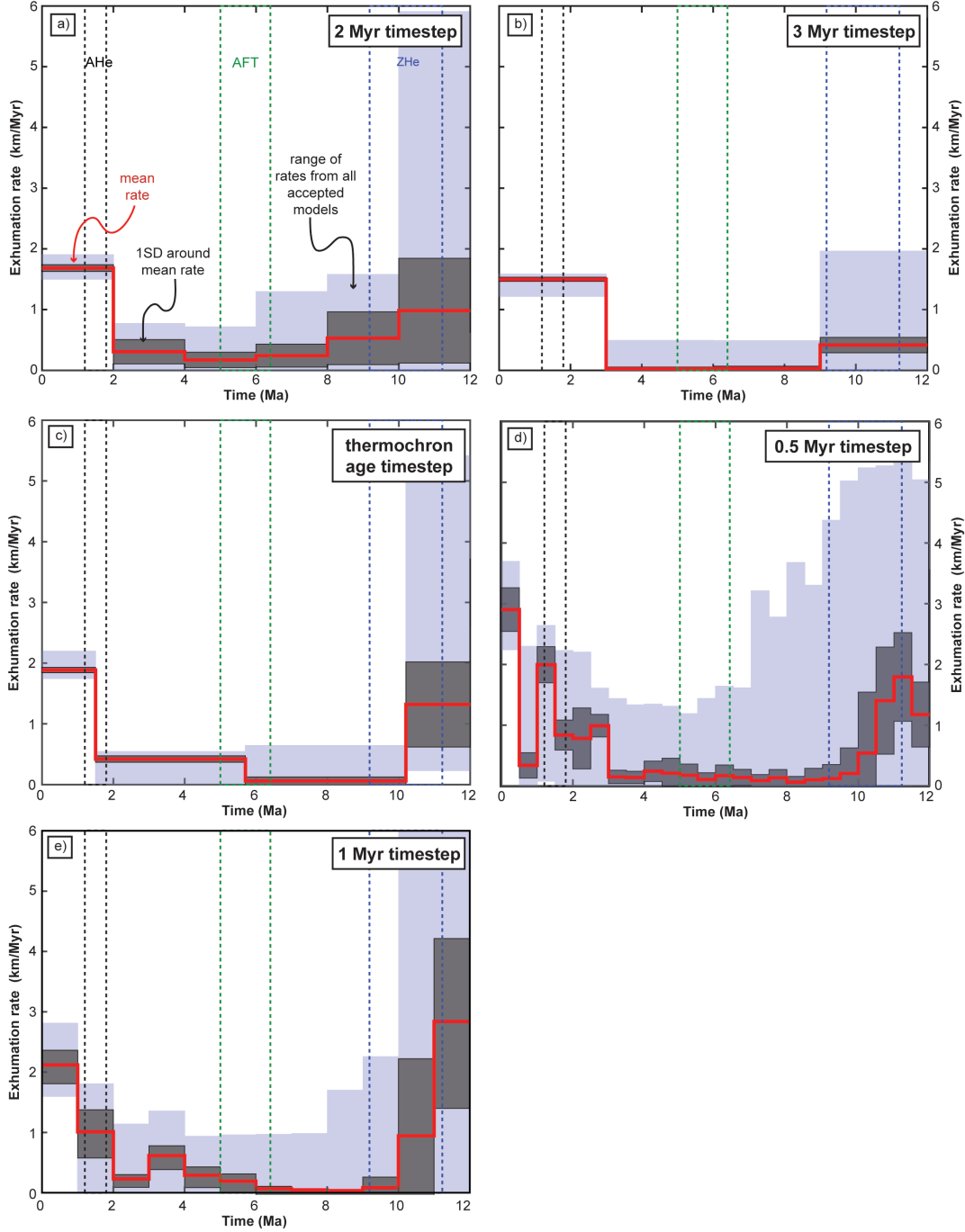


Figure S1: Outcomes from Pecube simulations investigating different time step durations for sample OP1513. Panels (a–d) display the exhumation rate histories for additional simulations using time steps of 2 Myr, 3 Myr, a duration defined by the thermochronometric ages of the sample, and 0.5 Myr, respectively. Panel (e) shows the exhumation rate history for a time step of 1 Myr, as already displayed in Figure 5 of the main manuscript. Dashed boxes indicate the cooling ages of AHe, AFT and ZHe with the respective uncertainty (1SD). For a detailed explanation of the modeling approach see Section 3.2 in the main manuscript.

S3 Additional information for flux steady-state analysis

S3.1 Sediment thickness during influx calculations

We calculated our influx volumes reported in Table 5 for three different sediment thicknesses, considering a pre-Quaternary thickness and present-day thickness as well as a possible increase in thickness occurring at 2 Ma. The sediment thickness of 2.5 km corresponds to the average present-day sediment thickness along the deformation front (Figure 3). The pre-Quaternary sediment thickness is difficult to determine for the entire 40 Myr duration of subduction and sediment accretion. However, we focused our analysis on the past 14 Myr, where we estimated the thickness by the following approach.

As displayed in Figure 3, the oceanic crust presently subducting is very young (~6–9 Ma). Together with the fast subduction rate of 34 km/Myr, which was even faster prior to 6 Ma (~60 km/Myr, Fig. 6), this prevents the accumulation of a thick succession of sediments on top of the oceanic crust. For instance, the pre-Quaternary sedimentation rates obtained from the ODP boreholes are around 80–110 m/Myr (Table 1). Assuming it takes the oceanic crust about 9 Myr to reach the deformation front (the oldest oceanic crust at the deformation front is currently 9 Ma old) would yield a sediment thickness of ~700–1000 m at the deformation front for the given sedimentation rate.

However, this is likely an underestimation of the actual thickness, because the inherent assumption for this calculation is that the spreading rate and convergence rate stay constant over time. Furthermore, the sedimentation rate likely increases with decreasing distance to the deformation front, because more detritus is delivered through submarine canyons and turbidity currents. Therefore, we suggest a minimum sediment

thickness of 1500 m for the pre-Quaternary as a good estimate of this otherwise difficult to constrain parameter.

S3.2 Creation of the sediment cross-sections

For calculation of the sediment volumes in the two cross-sections (Fig. 7), the lower boundary of the area occupied by the sediments corresponds to the top of the subducted slab, which is derived from the Slab1.0 model (Hayes et al., 2012; McCrory et al., 2012). Unfortunately, no uncertainty estimates are provided for this model. McCrory et al. (2012) only note that their current estimate of the top of the subducted slab locally differs by 5 km in the vertical dimension from results from prior studies. As the current study is the most comprehensive and up-to-date one, we use their results for our calculations.

The upper boundary is defined by the topography/bathymetry or the Hurricane Ridge Fault (HRF), the roof thrust separating the accreted sediments from the overlying Coast Range Terrane (CRT). At the surface, the location of the HRF is taken from a geologic map (Tabor and Cady, 1978) and at depth we use information provided by a seismic study (Calvert et al., 2011). This study provides seismic velocities at depths of 22 km and 34 km for the Olympic Peninsula (Figures 3b and c in the original publication of Calvert et al., 2011), where a distinct area of low seismic velocities (LVZ = low velocity zone) can be observed beneath the Olympic Mountains. Calvert et al. (2011) interpret this LVZ to correspond to accreted/underplated sediments, which are enclosed by material of higher seismic velocities (possibly the subducted oceanic crust below or basaltic rocks of the CRT on top of the sediments). Therefore, we assume that the eastern boundary of the

LVZ represents the HRF and contour the boundary between low and high velocities at depths of 22 km and 34 km. According to Calvert et al. (2011), the seismic velocities of the accreted sediments vary with latitude and range from 5.8–6.5 km/s (between 47.25°N and 48.1°N) and 6.7–7.0 km/s (north of 48.1°N). Hence, we mapped and contoured the boundary between sediments and CRT, distinguished by different velocities. The solid black line in Figure S2 is constructed using a seismic velocity of ~6.6 km/s (boundary between yellow and orange pixels in Figures 3b and c of Calvert et al., 2011), and we consider the volumes calculated with this outline as the most representative estimates. The cross-sections and volumes shown in Figure 7 correspond to this geometry (yielding values of 5348 km² and 3672 km² for Profile 1 and 2, respectively).

In order to provide an uncertainty for our calculated volumes, we also estimate the geometry of the HRF using different velocities. A maximum extent uses a velocity of ~7.0 km/s as boundary between sediments and CRT (boundary between bright and dark orange pixels in Figure 3b and c of Calvert et al., 2011), and a minimum extent uses a velocity of ~6.4 km/s as boundary (boundary between light green and yellow pixels in Figure 3b and c of Calvert et al., 2011). These maximum and minimum estimates for the sediment extent are shown as thin, dashed lines in Figure S2 for the respective depths of 22 km and 34 km.

The uncertainties in the location for the HRF reported in Figure 7 are based on these maximum and minimum extents. Volumes calculated with these extents yield values of 5186 km² and 5572 km² (Profile 1), and 3446 km² and 4005 km² (Profile 2). The uncertainties of the calculated sediment in Figure 7 are derived from these minimum/maximum extents, and correspond to 5–10% of the reported volume. In

general, the uncertainties of the location of the HRF at depth are largest in the southern part of the Olympic Peninsula (represented by the width of the dashed lines around the thick, solid line in Figure S2). Calvert et al. (2011) also note that the resolution of their reconstruction is reduced in the northern part of the peninsula, where velocities for the accreted sediments could be higher compared to areas in the south. Hence, we hesitate to construct a cross section for this part of the mountain range.

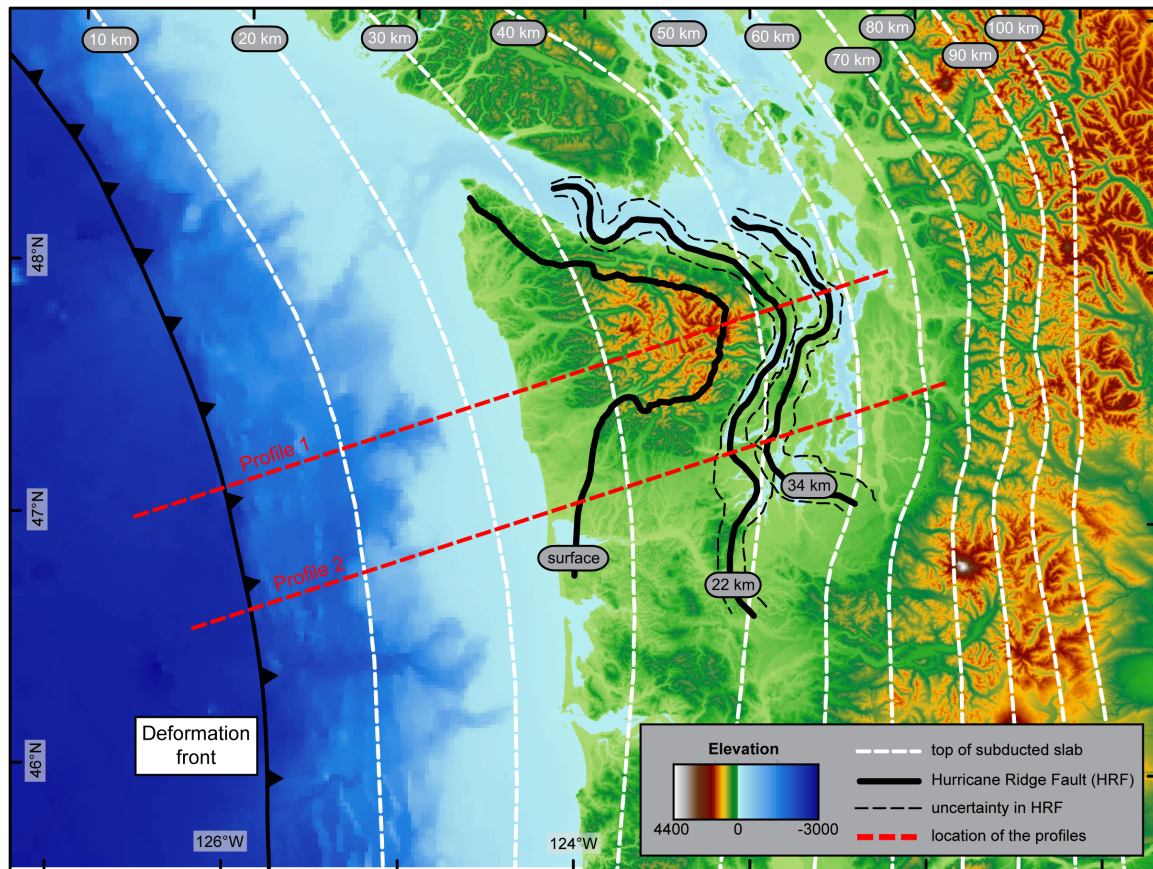


Figure S2: Map showing the data used for constructing Profile 1 and 2 (shown in Figure 7). Top of the subducted slab is taken from the Slab1.0 model (Hayes et al., 2012; McCrory et al., 2012). Trace of the Hurricane Ridge Fault (HRF) is taken from a geologic map at the surface (Tabor and Cady, 1978) and derived from the seismic study of Calvert et al., (2011) at depths of 22 and 34 km. The black dashed lines correspond to our estimates of uncertainty of the HRF at the respective depth. See Section S3.2 for details.

References

- Calvert, A. J., Preston, L. A. and Farahbod, A. M.: Sedimentary underplating at the Cascadia mantle-wedge corner revealed by seismic imaging, *Nat. Geosci.*, 4(8), 545–548, doi:10.1038/ngeo1195, 2011.
- Fitzgerald, P. G., Baldwin, S. L., Webb, L. E. and O’Sullivan, P. .: Interpretation of (U–Th)/He single grain ages from slowly cooled crustal terranes: A case study from the Transantarctic Mountains of southern Victoria Land, *Chem. Geol.*, 225(1–2), 91–120, doi:10.1016/j.chemgeo.2005.09.001, 2006.
- Flowers, R. M. and Kelley, S. A.: Interpreting data dispersion and “inverted” dates in apatite (U–Th)/He and fission-track datasets: An example from the US midcontinent, *Geochim. Cosmochim. Acta*, 75(18), 5169–5186, doi:10.1016/j.gca.2011.06.016, 2011.
- Hayes, G. P., Wald, D. J. and Johnson, R. L.: Slab1.0: A three-dimensional model of global subduction zone geometries, *J. Geophys. Res. Solid Earth*, 117(B1), doi:10.1029/2011JB008524, 2012.
- McCrory, P. A., Blair, J. L., Waldhauser, F. and Oppenheimer, D. H.: Juan de Fuca slab geometry and its relation to Wadati-Benioff zone seismicity, *J. Geophys. Res. Solid Earth*, 117(B9), doi:10.1029/2012JB009407, 2012.
- Tabor, R. W. and Cady, W. M.: The structure of the Olympic Mountains, Washington: Analysis of a subduction zone, US Govt. Print. Off., 1978.